Kevin M. Tharp,[1,2] Amit K. Jha,[2] Judith Kraiczy,[1] Alexandra Yesian,[1] Grigory Karateev,[4] Riccardo Sinisi,[4] Elena A. Dubikovskaya,[4] Kevin E. Healy,[2,3] and Andreas Stahl[1]

Matrix-Assisted Transplantation of Functional Beige Adipose Tissue

Diabetes 2015;64:3713–3724 | DOI: 10.2337/db15-0728

Novel, clinically relevant, approaches to shift energy balance are urgently needed to combat metabolic disorders such as obesity and diabetes. One promising approach has been the expansion of brown adipose tissues that express uncoupling protein (UCP) 1 and thus can uncouple mitochondrial respiration from ATP synthesis. While expansion of UCP1-expressing adipose depots may be achieved in rodents via genetic and pharmacological manipulations or the transplantation of brown fat depots, these methods are difficult to use for human clinical intervention. We present a novel cell scaffold technology optimized to establish functional brown fat–like depots in vivo. We adapted the biophysical properties of hyaluronic acid–based hydrogels to support the differentiation of white adipose tissue–derived multipotent stem cells (ADMSCs) into lipid-accumulating, UCP1-expressing beige adipose tissue. Subcutaneous implantation of ADMSCs within optimized hydrogels resulted in the establishment of distinct UCP1-expressing implants that successfully attracted host vasculature and persisted for several weeks. Importantly, implant recipients demonstrated elevated core body temperature during cold challenges, enhanced respiration rates, improved glucose homeostasis, and reduced weight gain, demonstrating the therapeutic merit of this highly translatable approach. This novel approach is the first truly clinically translatable system to unlock the therapeutic potential of brown fat–like tissue expansion.

The unabated growth of the obesity epidemic and associated diseases such as type 2 diabetes reflects the current lack of effective strategies for intervention and treatment. Since obesity results from an imbalance in the ratio of energy intake to energy expenditure, it can be treated with reduced caloric uptake and/or increasing energy expenditure. Brown adipose tissue (BAT) and inducible brown-like cells in white adipose tissue (WAT), currently referred to as beige or brite adipocytes (1), possess the innate ability to dissipate metabolic energy as heat through nonshivering thermogenesis. This is possible owing to the presence of the uncoupling protein (UCP) 1 (2), a long-chain fatty acid anion/proton symporter (3), in the inner mitochondrial matrix, which allows the return of protons after they have been pumped across the mitochondrial inner membrane by the electron transport chain, thereby bypassing ATP synthase. While the importance of BAT for thermogenesis in smaller mammals and human infants has been well documented (4), only recent observations have demonstrated the presence of BAT in adult humans (5,6). These observations have reversed the dogma that BAT is absent in adult humans and have presented a new route for the treatment of obesity-related disorders. Over 90% of the metabolic energy consumed by activated BAT will be derived from the β-oxidation of free fatty acids (FFAs) (7). Furthermore, many studies have suggested that the amount of BAT correlates inversely with BMI, raising the possibility that variations in the amount of BAT may drive alterations in body weight (8). Thus, increasing BAT mass may serve as a novel approach to combat obesity and related disorders such as type 2 diabetes. This concept is supported by recent studies that found evidence for metabolic enhancement, including the reversal of type 1 diabetes (9) and resistance to diet-induced obesity, in mouse models of BAT expansion (10) via transplantation of existing BATs.

[1]Graduate Program in Metabolic Biology, Department of Nutritional Sciences & Toxicology, University of California, Berkeley, Berkeley, CA
[2]Department of Bioengineering, University of California, Berkeley, Berkeley, CA
[3]Department of Materials Science & Engineering, University of California, Berkeley, Berkeley, CA
[4]Institute of Chemical Sciences and Engineering, École Polytechnique Fédérale de Lausanne, Lausanne, Switzerland

Corresponding author: Andreas Stahl, astahl@berkeley.edu, or Kevin E. Healy, kehealy@berkeley.edu.

Received 1 June 2015 and accepted 21 July 2015.

This article contains Supplementary Data online at http://diabetes.diabetesjournals.org/lookup/suppl/doi:10.2337/db15-0728/-/DC1.

Strategies for expanding BAT can be grouped into two general categories: pharmaceutical/genetic intervention to trigger endogenous BAT/beige differentiation pathways and the ex vivo generation of BAT for implantation (11–15). Gene therapy approaches, for example, the ectopic overexpression of the transcriptional regulator PRDM16 (14,16), are powerful tools to investigate BAT biology but are difficult to apply clinically owing to the risks associated with current gene therapy regiments (17). Pharmacological activation of differentiation pathways that drive a WAT-to-BAT transition ("browning") run the risk of affecting the function of other tissues and offer little control over the location and temporal extent of BAT expansion. Similarly, heterologous transplantation of existing BAT into immunecompromised recipients has demonstrated the metabolic impact of BAT expansion (10), but this approach has no clinical translatability owing to a paucity of donor tissues and the expected host-versus-graft rejection. Thus, we propose an alternative approach that takes advantage of current progress in the field of bio-inspired hyaluronic acid (HyA) hydrogels to engineer a matrix-assisted cell transplantation (MACT) system for beige adipose tissue (BAT-MACT) derived from the readily available, multipotent stem cell (MSC)-containing, stromal vascular fraction of WAT (18).

RESEARCH DESIGN AND METHODS

Animals and Diets

Experiments were performed according to Association for Assessment and Accreditation of Laboratory Animal Care guidelines and approved by the University of California, Berkeley, Animal Care and Use Committee. Eight-week-old male C57BL/6J or FVB/NJ mice (The Jackson Laboratory) were group housed for a 1-week acclimation period (temperature 21 ± 2°C, humidity 30–70%) in Tecniplast cages filled with sani-chip bedding (Harlan) and then individually housed 1 week prior to implantation and administration of high-fat (60%) diet (Teklad TD.06414). Luciferase-expressing L2G85 (FVB/NJ) mice were used as a cell source for experiments using bioluminescent monitoring of implant viability and function.

Adipose-Derived MSC Isolation

Fat depots from L2G85 (FVB/NJ) or C57BL/6J mice, perigonadal (visceral) or inguinal (subcutaneous), respectively, were isolated from 3-month-old mice as previously described (19).

In Vitro Differentiation of Adipose-Derived MSCs

Adipose-derived MSCs (ADMSCs) (initial density ~100 k cells/cm^2) were cultured to postconfluence on tissue culture polystyrene (TCPS) or adsorbed peptide surfaces. Differentiation was induced for 3 days with 0.85 μmol/L insulin, 10 nmol/L triiodothyronine, 1 μmol/L dexamethasone, and 500 μmol/L isobutylmethylxanthine in high-glucose DMEM (Invitrogen) with 10% FCS (Gibco) and penicillin/streptomycin (P/S) (Gibco). The induced cells were then treated with 0.85 μmol/L insulin and 100 nmol/L rosiglitizone in high-glucose DMEM (Invitrogen) with 10% FCS and P/S for 12 subsequent days. Before harvest with TRIzol, cultures were treated with 5 μg/mL CL-316243 for 4 h. The initial peptide screening differentiation experiments were carried with the goal of determining the differentiation outcome of an adhesion-selected cell fraction, a process referred to as "panning." To this end, primary ADMSCs were given 4 h to adhere onto the surface coating, cultures were then PBS washed twice to remove less adherent cells within the ADMSC population, and differentiation was induced as described above (Fig. 1*A–C*). Experiments to determine optimal proportions of selected peptides were carried out without washing off poorly adherent cells (Fig. 1*D–F*).

Immunohistochemistry

Immunohistochemistry was performed as previously described (20). Whole in vitro hydrogels were fixed with 4% paraformaldehyde for 30 min at room temperature and imaged within their MilliCell insert (Milipore) placed on coverslips.

mRNA

Tissue samples were suspended in RNAlater ICE (Ambion) and stored at −20°C. mRNA was isolated from RNAlater ICE stabilized tissues or directly from in vitro cultures of monolayers or cell-laden hydrogels with TRIzol reagent (Ambion). Tissue samples were homogenized with a Polytron PT 2100. Assays were carried out on an ABI 7500 RT-PCR system with TaqMan Universal Master Mix II and validated PrimeTime primer probe sets (Integrated DNA Technologies). A first-strand cDNA synthesis kit (Fisher) was used to transcribe 5 μg RNA/20 μL. cDNA (100 ng) was used per RT-PCR reaction in triplicates. The Δ-Δ-CT method was used to comparatively assess mRNA quantity. All data are represented as a sample's value normalized to GAPDH relative to source tissue–derived ADMSCs, source tissue, or endogenous BAT.

Protein Quantification and Western Blotting

A Pierce BCA kit was used to measure protein concentrations. Western blotting was accomplished with Novex 4–20% tris-glycine gels, iBlot Transfer Stacks (Invitrogen), and a LI-COR Odyssey infrared imager with anti-UCP1 (Sigma-Aldrich) and anti–β-tubulin E7 clone (Developmental Studies Hybridoma Bank). Data are presented as UCP1 normalized to β-tubulin relative to endogenous BAT.

Synthesis of HyA Hydrogels

Modified HyA (500 kDa) was synthesized using previously established methods (21). The acrylated HyA (AcHyA)-C16 or AcHyA-Ag73 was synthesized by reacting peptides (CGGKAFDITYVRLKF [10 mg] or CGGRKRLQVQLSIRT [10 mg]) with AcHyA (25 mg, 10 mL deionized water) at room temperature. To synthesize hydrogels, we dissolved AcHyA (2 mg), AcHyA-C16 (6 mg), and AcHyA-Ag73 (2 mg) in 0.3 mL triethanolamine buffer (0.3 mol/L, pH 8), incubated for 30 min at 37°C, and subsequently matrix metalloprotease (MMP-13)–cleavable peptide (CQPQGLAKC) (3 mg in 50 μL triethanolamine buffer) was added to HyA peptide solution. The crosslinker concentration was varied to achieve complete crosslinking of available acrylate

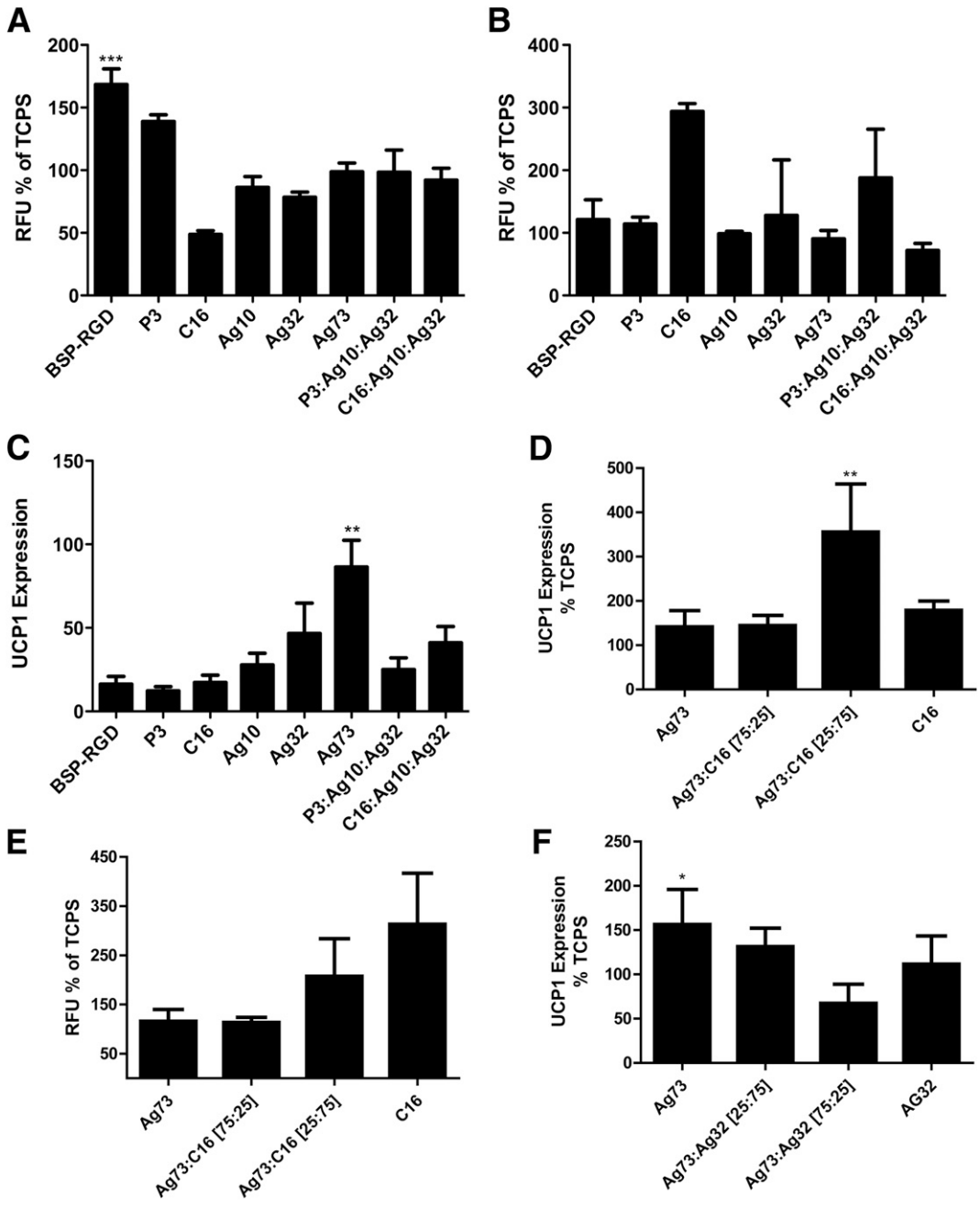

Figure 1—Effects of adhesion ligands on ADMSC differentiation. *A*: Adhesion of ADMSCs to adsorbed peptides after 4 h incubation; relative fluorescent units (RFUs) of adherent cells (n = 3). *B*: Neutral lipid staining of ADMSCs after differentiation on indicated adhesion ligands (n = 3). *C*: UCP1 mRNA expression of WAT-derived murine ADMSCs that were differentiated on indicated adhesion substrate–coated TCPS relative to undifferentiated ADMSCs (n = 3). *D*: UCP1 mRNA expression of WAT-derived ADMSCs differentiated on mixtures of Ag73 and C16 relative to differentiated ADMSCs on TCPS (n = 6). *E*: Neutral lipid staining of WAT-derived ADMSCs on varied mixtures of Ag73 and C16 relative to differentiated ADMSCs on TCPS (n = 6). *F*: UCP1 mRNA expression of WAT-derived ADMSCs differentiated on mixtures of Ag73 and Ag32 relative to differentiated ADMSCs on TCPS (n = 6). Significance at $^{*}P < 0.05$, $^{**}P < 0.01$, and $^{***}P < 0.001$.

functionalities on the HyA macromers (~200 mmol/L). The initial storage modulus of all hydrogels (in vitro and in vivo) was measured consistently to be ~850 Pa.

BAT-MACT Generation

ADMSCs were cultured in vitro in DMEM with 10% FBS and 1% P/S on TCPS. Two days postconfluency, differentiation was induced with 0.85 μmol/L insulin, 10 nmol/L triiodothyronine, 1 μmol/L dexamethasone, and 500 μmol/L isobutylmethylxanthine (for white adipocytes scaffolded by unmodified AcHyA [WAT-MACT], triiodothyronine was omitted from the cocktail). Three million cells per mL were suspended in AcHyA-Ag73:C16 (1:3 molar ratio) just before implantation (for WAT-MACT, cells were suspended in AcHyA).

The cell suspension was mixed with the MMP-13–cleavable crosslinker at a final concentration of ~200 mmol/L (sufficient to achieve a modulus of ~850 Pa) and 100 μL of the forming BAT-MACT was immediately injected to recipient mice.

Experiments where bioluminescent imaging (BLI) was used to monitor the viability and function of the BAT-MACTs, in conjunction with metabolic measures, were performed in FVB/NJ mice with ADMSCs isolated from perigonadal fat depots of syngenic L2G85 donor mice. Experiments where metabolic parameters were assessed without BLI monitoring were performed with C57BL/6J mice implanted with BAT-MACTs generated with ADMSCs isolated from the inguinal adipose depot.

In Vitro BAT-MACT

ADMSCs were cultured in vitro in DMEM with 10% FBS and 1% P/S on TCPS. Three million subconfluent cells per milliliter were suspended in the specific hydrogel and injected into a Millicell transwell chamber (Millipore) in a 24-well tissue culture plate (Falcon). After 2 days of culture in DMEM with 10% FBS and 1% P/S, the differentiation protocol described for the in vitro differentiation of ADMSCs was implemented.

BLI

Imaging was accomplished with an IVIS Spectrum. Luciferin (45 μL; 4 mg/mL i.p.) in PBS was injected into animals. FFA-SS-Luc 100 μL of (1.4 μg/μL) intraperitoneal compound was injected into mice. Once the BLI signal dropped off (~40 min), the animals were removed to recover. Four hours later, once all original BLI signal was extinguished, 1 μg CL-316243/g body wt i.p. was injected followed by another dose of the FFA-SS-Luc.

Respirometry

Respirometry was performed with the Comprehensive Lab Animal Monitoring System (CLAMS) (Columbus Instruments). Measurements were taken over 24-h periods, and average values were assessed (22). CL-316243 was administered to animals, and the 4-h preinjection was compared with the 4-h postinjection time periods. Activity was monitored in 1-min intervals of infrared beam breaks in *x*-, *y*-, and *z*-axes and was found to be not significantly different for any of the groups.

Serum Cytokine Measurements

A Bio-Rad Bio-Plex Pro Mouse Cytokine 23-Plex immunoassay kit was used per the manufacturer's instructions with a Bio-Rad MAGPIX system.

Rheology

Viscoelastic properties of the hydrogel were determined using an oscillatory rheometer with parallel-plate geometry (8 mm) and a gap height of 0.2 mm under 10% constant strain and frequency ranging from 0.1 Hz to 10 Hz at 37°C in a humidity-controlled chamber.

Cell Adhesion Assays

Purified peptides were suspended at 20 μmol/L in ultrapure water with 1% P/S. Peptide suspensions (20 μmol/L) were allowed to adsorb to the 24-well TCPS plates (BD Falcon) overnight at 4°C. Plates were then washed two times with PBS. Twenty thousand primary ADMSCs suspended in DMEM with 10% FBS and 1% P/S were added to each well and incubated at 37°C for 4 h. Media and nonadherent cells were removed and centrifuged to separate the cells from media. The adherent and nonadherent cells were then counted with the CyQUANT kit (Invitrogen).

Cold Challenge and Core Body Temperature

A Physitemp BAT-12 Microprobe thermometer was used to measure core body temperature of mice rectally. Cold challenges took place in a 4°C walk-in refrigerator approved for use in accordance with Association for Assessment and Accreditation of Laboratory Animal Care guidelines.

Serum Glucose and Glucose Tolerance Tests

Blood glucose was measured with a Nova Max blood glucometer and Nova Max glucose test strips (Sanvita). Mice were injected with an equivalent dose of glucose (167 μL of 300 g/L glucose). This dose was selected as a dose that the median mouse weight would warrant to achieve the standard glucose dose of 2 mg/g body wt generally used for a glucose tolerance test.

Statistical Analysis

All data are presented as SEM analyzed using Prism (GraphPad). Statistical significance was determined by either one-way ANOVA followed by Tukey posttest or unpaired two-tailed Student *t* test. Significance presented at $P < 0.05$, $P < 0.01$, and $P < 0.001$.

RESULTS

Adhesion Ligands Enhance Beige Fat Differentiation

Cell adhesion and matrix interactions exert significant control over MSC differentiation (23); however, no screens have examined how these interactions affect the browning of WAT-derived MSCs (ADMSCs). To this end, ADMSCs were extracted from WAT (19) and cultured on TCPS plates coated with specific peptides found to be ligands for integrins and syndecans (Fig. 1*A* and Supplementary Table 1). Differentiation was induced, and lipid droplet accumulation (Fig. 1*B*) and UCP1 expression were assessed (Fig. 1*C*). Our initial screens identified non-RGD peptide sequences such as AG73 (CGG**RKRLQVQLSIRT**), an adhesion ligand for α_6 integrins and syndecan-1 (24,25), as particularly efficient in driving UCP1 expression of ADMSCs, while **C16** (CGG**KAFDITYVRLKF**), an $\alpha_{5/v}\beta_{1/3}$ integrin–engaging ligand (26), induced lipid accumulation. Interestingly, while all peptide-coated substrates outperformed uncoated TCPS in UCP1 expression assays, a combination of AG73 with C16 (1:3 molar ratio) had significant effects on UCP1 expression (Fig. 1*D* and *E*). Combining varied concentrations of AG73 with AG32 (CGG**TWYKIAFQRNRK**), another $\alpha_6\beta_1$ integrin–engaging ligand (25), we observed attenuated UCP1 expression (Fig. 1*F*). The impressive enhancement of UCP1 expression

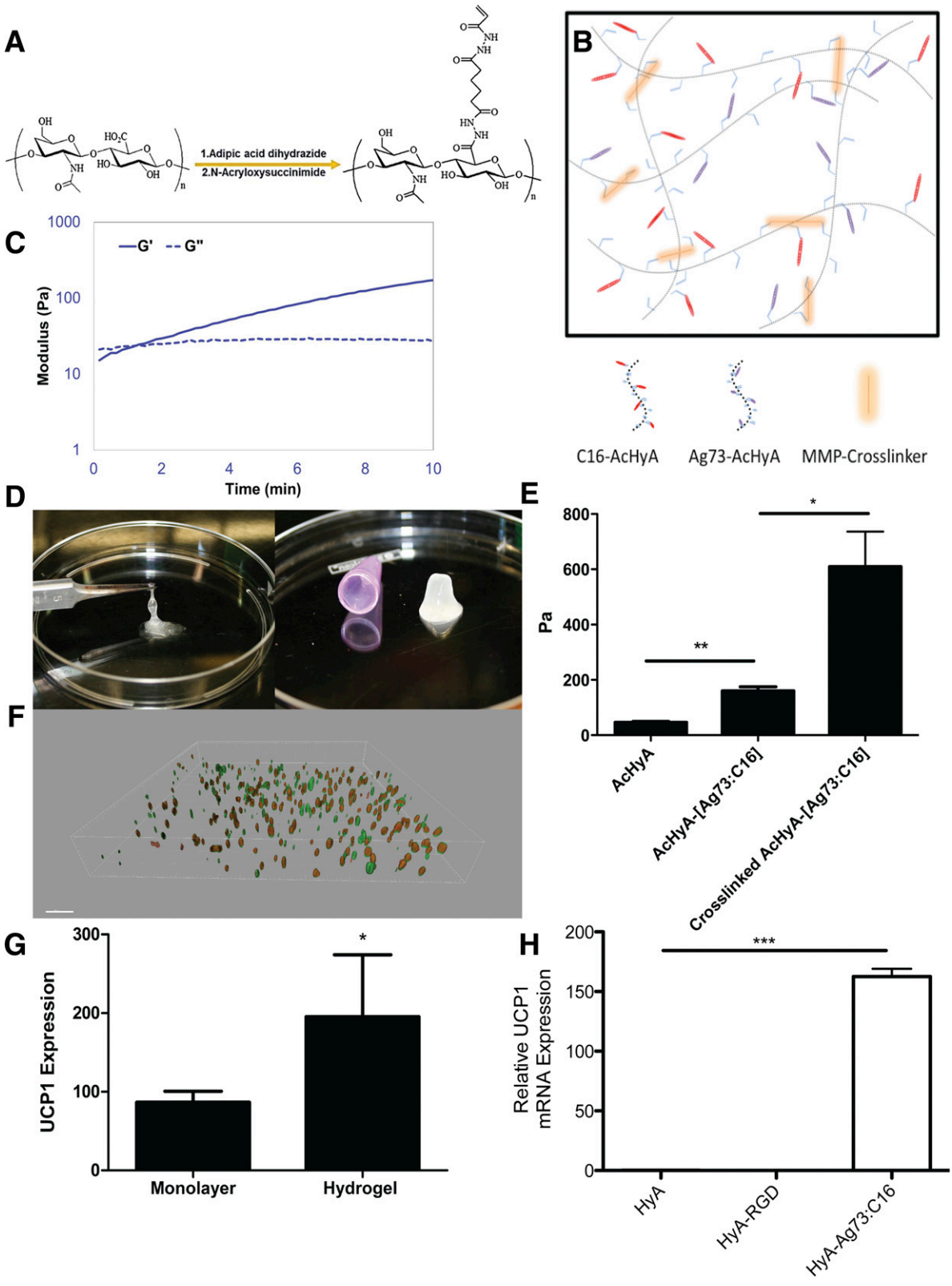

Figure 2—Bio-inspired HyA hydrogels. *A*: Schematic of the synthesis of AcHyA by sequential conjugation of adipic acid dihydrazide and N-acryloxysuccinimide. *B*: Representation of the assembly of optimized hydrogel through crosslinking of C16-AcHyA to Ag73-AcHyA macromers with an MMP-degradable crosslinker (not to scale). *C*: Time line of HyA hydrogel gelation. Gelation was considered complete when the storage modulus (G′) exceeded the loss modulus (G′′) (measured in Pascals). *D*: Photographs of AcHyA before (left) and 5 min after (right) the addition of the crosslinker. *E*: Storage modulus of ADMSC suspended in uncrosslinked and crosslinked hydrogels cultured in vitro after 72 h (n = 3). *F*: Three-dimensional reconstruction of in vitro ADMSCs in optimized hydrogel (red, UCP1; green, MitoTracker) after completion of differentiation. *G*: UCP1 expression of differentiated ADMSCs with the optimized peptide mixture in monolayer and

achieved by optimizing adhesion ligands is highlighted by the fact that previous attempts to differentiate WAT-derived MSCs into BAT yielded UCP1 levels significantly lower than BAT-derived MSCs (11). In contrast, we find UCP1 expression in WAT-derived MSCs differentiated on optimized adhesion ligands to be comparable with those of differentiated BAT-derived MSCs in vitro (Supplementary Fig. 1).

Optimized Hydrogel Provides Instructive Microenvironment for Beige Fat

Engagement with the extracellular matrix provides a crucial factor in driving MSC differentiation through biophysical properties and composition (27–29). Using our expertise in biomaterials (20,30–32), we synthesized AcHyA macromers (Fig. 2*A*) conjugated with the bioactive peptides. These functionalized AcHyA macromers (AcHyA-Ag73 and AcHyA-C16) were combined with specific MMP-sensitive peptide crosslinkers at defined concentrations to form hydrogels with precise physical characteristics and degradation kinetics (Fig. 2*B*). The synthesis of hydrogel networks takes advantage of the Michael-type addition reaction (i.e., attack of the acrylate group by available cysteine thiols to form a covalent bond) (33,34), which forms a defined hydrogel scaffold within 5 min (Fig. 2*C* and *D*).

We verified that the ADMSCs embedded in the optimized matrix were forming functional cell adhesions with the hydrogel. By suspending ADMSCs in uncrosslinked AcHyA-Ag73:C16 or unmodified AcHyA, we found that the inclusion of adhesion peptides resulted in a significant increase in the storage modulus of uncrosslinked hydrogels seeded with ADMSCs, indicating that the adhesion peptides enable cells to mechanically integrate the synthetic extracellular matrix (Fig. 2*E*). The optimized hydrogel scaffold allowed the ADMSCs to evenly distribute and differentiate into UCP1-positive adipocytes in vitro without direct cell-cell contact (Fig. 2*F* and Supplementary Fig. 2). Importantly, culturing cells in AcHyA-Ag73:C16 hydrogels significantly improved UCP1 expression of differentiated ADMSCs in vitro compared with monolayers exposed to adsorbed Ag73:C16 (Fig. 2*G*). Notably, unconjugated hyaluronan- or RGD (CGGNGEP**RGD**TYRAY)-conjugated hydrogels were not capable of inducing UCP1 expression independent of Ag73 and C16 (Fig. 2*H*).

To produce a functional BAT-MACT, we isolated ADMSCs from donor WAT, initiated differentiation in vitro, and suspended the cells in Ag73 and C16 presenting AcHyA macromers. BAT-MACTs were formed by mixing cells ($3*10^6$/mL) with AcHyA macromers (3 wt%) and a MMP-13–sensitive crosslinker. The cell suspension was immediately injected with a 22.5-gauge needle into the subcutaneous inguinal fat pad (or as noted) of recipient animals. The viability of the implanted BAT-MACT was monitored via bioluminescence using luciferase-expressing donor cells delivered in a hydrogel or suspended in PBS. Subcutaneous injections of luciferin adjacent to the implant demonstrate luminescence for both conditions after implantation. Importantly, the PBS-delivered ADMSCs produce little luminescence when the bioluminescent substrate is introduced into general circulation. By delivering luciferin with intraperitoneal injections distant from the BAT-MACT implant site, we observed massive signal expansion during the first week, which declines to undetectable levels 4 weeks postimplantation (Fig. 3*A*).

Owing to the rapid crosslinking kinetics, BAT-MACTs form a distinct subcutaneous lobe upon injection that is clearly brown/beige in appearance (Fig. 3*B*). BAT-MACTs were highly vascularized on a macroscopic level, and thin sections of implants demonstrated an extensive and consistent vascular network throughout the implants (Fig. 3*C*). Likewise, UCP1-positive and lipid droplet–accumulating cells were evenly spread throughout the BAT-MACT (Fig. 3*D*). Interestingly, regions of the implant showed positive staining for tyrosine hydroxylase, the rate-limiting enzyme in the synthesis of catecholamines (Supplementary Fig. 3). Tyrosine hydroxylase is essential for the production of norepinephrine by sympathetic neurons and macrophages to not only activate respiration but also maintain differentiation status and function (35). UCP1 mRNA expression of the implanted MACT was >10-fold higher than that of comparable in vitro cultured MACTs (Fig. 3*E*) and reached 7–17% of the levels found in endogenous BAT (Supplementary Fig. 4). Importantly, PRDM16 and PPARγ expression in BAT-MACTs were comparable with those in endogenous BAT (Fig. 3*F*), highlighting the potential of the MACT.

Immense differences of UCP1 induction within white fat depots have been shown to be under genetic control (36). We confirmed these differences by generating BAT-MACTs from FVB/NJ and C57BL/6J mice. Similar to previously published findings, C57BL/6J visceral fat depots produce significantly less UCP1 protein than FVB/NJ or subcutaneously sourced C57BL/6J ADMSCs within our BAT-MACT system (Fig. 3*G*). To assess the effect of implant location, we analyzed two different implant sites in the thoracic and inguinal regions for lipid droplets and UCP1 expression. In BAT-MACTs from both implantation sites, we observed multilocular lipid droplets, UCP1-positive cells, and blood vessels with no apparent difference between the implantation sites. Impressively, UCP1 protein levels in both BAT-MACT sites reached ~30% of BAT from the same animals (Fig. 3*H*). Importantly, inflammatory cytokines measured in serum were not upregulated whatsoever by the BAT-MACT system; in fact, interleukin-2

comparable hydrogel (n = 4). *H*: ADMSCs differentiated in unconjugated HyA hydrogels, RGD-conjugated hydrogels, and Ag73:C16-conjugated hydrogels. GAPDH normalized UCP1 mRNA expression relative to WAT (n = 5). Significance at $^*P < 0.05$, $^{**}P < 0.01$, and $^{***}P < 0.001$.

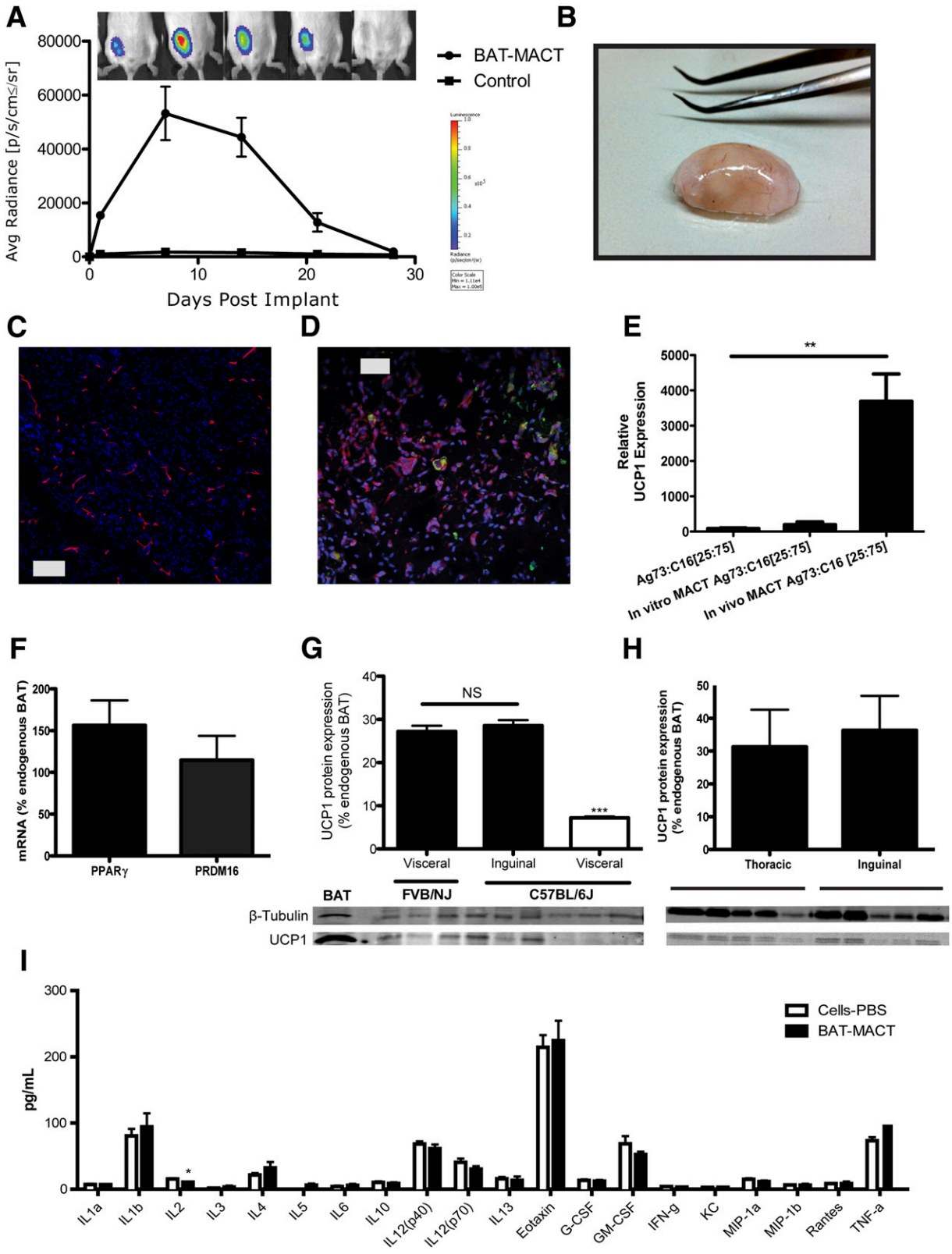

Figure 3—BAT-MACT in vivo characteristics. *A*: Persistence of BAT-MACT over time monitored by luciferase activity in live animals (FVB/NJ; n = 5); false color heat scale image indicating average (Avg) photon radiance. Max, maximum; Min, minimum; sr, steradian. *B*: Macroscopic morphology of implants after 2 weeks. BAT-MACTs were removed after 14 days; fixed, cryosectioned, and stained with DAPI; and stained for the vascularization marker endomucin (*C*) or neutral lipids (green) and UCP1 (red) (*D*). *E*: mRNA expression of UCP1 relative to WAT using samples from differentiated ADMSCs plated on Ag73 and C16 peptide-coated TCPS or in Ag73- and C16-conjugated AcHyA hydrogels cultured in vitro or implanted into recipient animals (FVB/NJ; n = 4, 3, or 6, respectively). *F*: PRDM16 and PPARγ mRNA expression normalized to GAPDH of BAT-MACTs after 2 weeks in vivo relative to endogenous BAT (FVB/NJ; n = 9). *G*: UCP1 protein

was dissipated (Fig. 3*I*). Therefore, the BAT-MACT system allows for the measurement of metabolic effects independent of inflammatory artifacts.

Beige Fat Implantation Enhances Metabolic Profiles of Recipients

To determine the metabolic impact of BAT-MACTs, we examined the respiratory capacity of animals augmented with a BAT-MACT or WAT-MACT. HyA matrixes have been shown to aid in the development and persistence of WAT (37,38), and WAT-MACTs formed fatty implants that were well vascularized, contained extensive lipid stores, and had undetectable UCP1 expression (Supplementary Fig. 5). The BAT-MACT implanted animals displayed significantly enhanced VO_2 and reduced respiratory exchange ratio, recapitulating the elevated fatty acid utilization and respiration after classical BAT activation (Fig. 4*A* and *B*). Furthermore, BAT-MACT augmented animals were significantly more responsive to CL-316243, a β_3-specific adrenergic agonist (Fig. 4*C*). To verify that FFAs would be taken up by BAT-MACTs, we used a recently developed optical probe for fatty acid uptake (39) and observed that an intraperitoneal injection of the probe was robustly taken up by BAT-MACTs. Importantly, as previously shown for endogenous BAT (40), injection of a β_3-adrenergic agonist significantly enhanced fatty acid uptake rates by the BAT-MACTs (Fig. 4*D*).

To test the impact of BAT-MACTs on thermogenesis, we examined core body temperature at room temperature (21°C) and over 24 h of 4°C. Body temperatures of BAT-MACT recipients were higher throughout the cold challenge as well as at room temperature (Fig. 4*E*). Thermography revealed that the implant is distinctly thermogenic (Supplementary Fig. 6). Importantly, this thermogenic effect was dependent on the amount of cells implanted (Fig. 4*F*) and the environmental temperature (Fig. 4*G*). Using C57BL/6J mice as a model for diet-induced obesity, we measured the impact of BAT-MACT impact on weight gain and glucose homeostasis. Animals implanted with BAT-MACTs and housed at 21°C for 2 weeks gain significantly less weight when fed a 60% fat diet compared with PBS-delivered ADMSCs, cell-free matrix, or WAT-MACTs (Fig. 5*A*) in spite of slightly higher food consumption (Fig. 5*B*). Extended monitoring of weight gain identified that the reduction of weight gain was significant within 2 weeks post–BAT-MACT implantation and concomitant high-fat feeding. The difference in weight gain was sustained over a time period coinciding with the lifetime of the BAT-MACT cells as measured by bioluminescence (Fig. 5*C*).

After 2 weeks, serum triglyceride levels were found to trend lower and serum free fatty acids were reduced in animals augmented with BAT-MACTs (Fig. 5*D* and Supplementary Fig. 7). Accompanying the reduced weight gain and serum FFAs, resting blood glucose levels (Fig. 5*E*) and glucose tolerance (Fig. 5*F*) were improved in BAT-MACTs but not WAT-MACTs, cell-free implants, or matrix-free implants of BAT-like cells.

DISCUSSION

Expansion of UCP1-positive tissue holds exciting potential to combat obesity and related disorders (41). However, few practicable approaches for clinical deployment have been presented thus far. This novel strategy to integrate WAT-derived MSCs with bioactive hydrogels bespoke to enhance differentiation, support tissue formation, and survival upon implantation provides the required core technology for autologous expansion of BAT mass in patients. ADMSCs are easily extractable and abundant and are already used in regenerative medicine (18). ADMSCs used in this study were only partially purified; further gains in differentiation effectiveness could be anticipated by sorting for UCP1-enriching markers such as Sca-1 (13), CD24, CD29 (15,42), and CD137 (43).

Hydrogel-based therapies are minimally invasive therapeutic options that will complement pharmacological and cell-based approaches (44). We selected HyA as the core scaffold of our matrix for its biocompatibility, biodegradability, and nonimmunogenic properties and its role in tissue development and repair (30). Recently, HyA has been shown to augment integrin-mediated mechanotransductive signaling (45) and likely plays an essential role in the overall effect that our matrix has on the differentiation of ADMSCs. Similar hydrogel systems have been proposed for clinical use that used crosslinkers and adhesion ligands that directly compete for attachment to the available functional groups on core polymeric chains within the hydrogel. These systems have struggled with compromised crosslinking efficiencies, unbound adhesion ligands preventing cell association with the matrix, and low–molecular weight core structures that degrade too rapidly to be useful (46).

Matrix stiffness plays an important role in cell fate determination and should be a critical design feature of cell transplantation systems (27). We have developed a modular hydrogel system that allows for modulus and biological properties of the hydrogel to be tuned independently. This modular approach to tissue engineering may be essential to target an optimal net modulus for the development and maintenance

expression of BAT-MACTs generated with ADMSCs from visceral or subcutaneous FVB/NJ or C57BL/6J mice 2 weeks postimplantation into a syngenic recipient relative to endogenous BAT ($n = 3$). NS, not significant. *H*: UCP1 protein expressed in BAT-MACTs of different implant sites after 2 weeks in vivo relative to endogenous BAT (FVB/NJ; $n = 5$). *I*: Serum cytokine levels measured 2 weeks postimplantation of BAT-MACT or the same ADMSCs delivered via PBS. Animals were administered the 60% fat diet for the duration of this study (C57BL/6J; $n = 6$). IL, interleukin. Significance at $^{**}P < 0.01$ and $^{***}P < 0.001$.

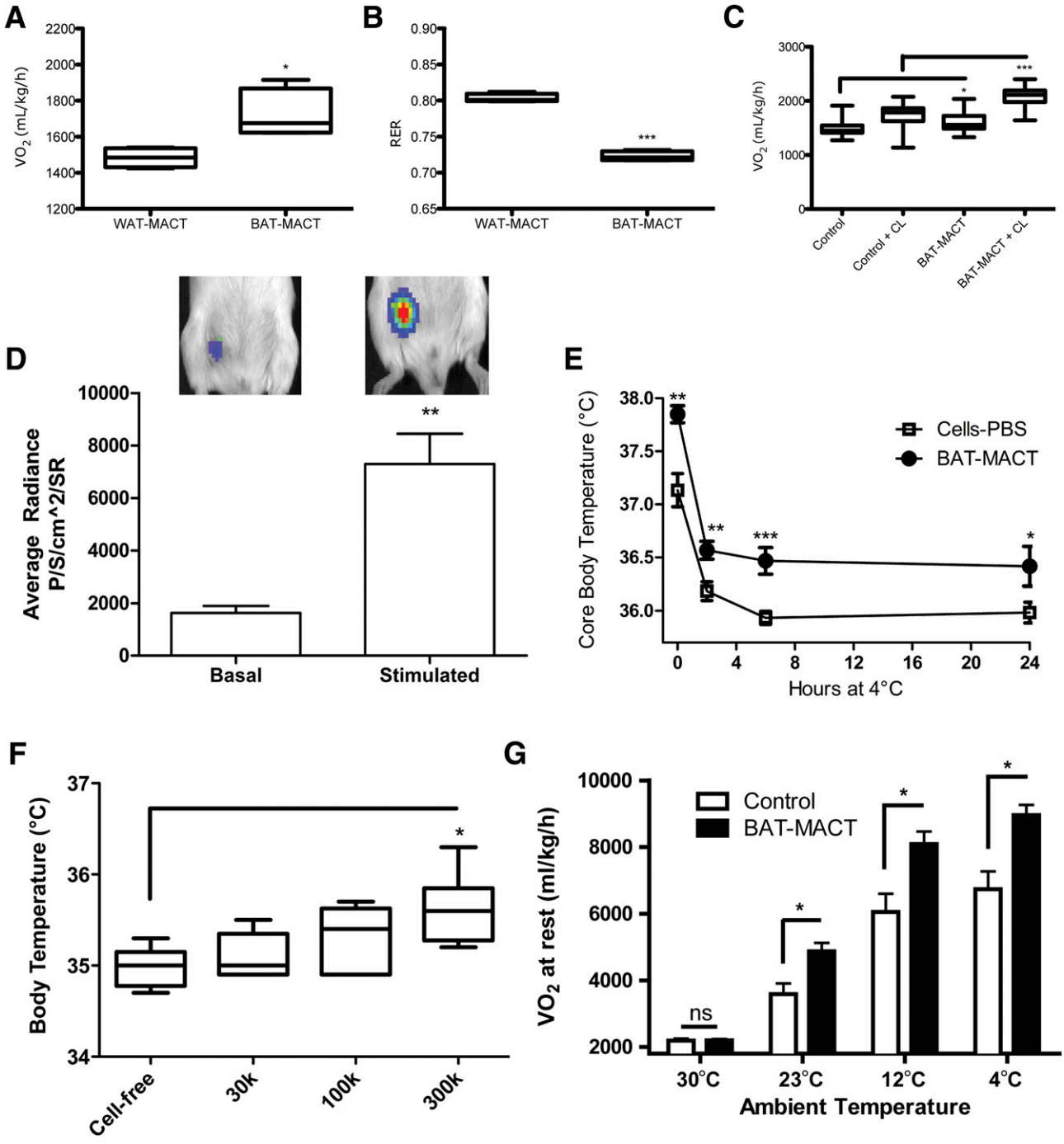

Figure 4—Metabolic effects of BAT-MACTs 2 weeks postimplantation. *A*: Average VO_2 rate over 24 h (FVB/NJ; $n = 4$). *B*: Average respiratory exchange ratio (RER) over 24 h (FVB/NJ; $n = 4$). *C*: Average VO_2 rate 4 h before and after β-adrenergic agonist CL-316243 (CL) was administered (FVB/NJ; $n = 4$). *D*: Fatty acid uptake of BAT-MACTs under basal and CL-316243–stimulated conditions (FFA-SS-Luc) (FVB/NJ; $n = 3$). SR, steradian. *E*: Core body temperature during a 24-h cold challenge (4°C) (FVB/NJ; $n = 6$). *F*: Core body temperature after a 6-h cold challenge (4°C) of animals implanted with the indicated number of ADMSCs in 100 μL optimized hydrogels on a normal chow diet (FVB/NJ; $n = 6$). *G*: Average VO_2 rate of mice implanted with BAT-MACT or comparable cells delivered in PBS during the 10–14 days postimplantation in a temperature-controlled CLAMS unit (C57BL/6J; $n = 4$). Explanation of controls: WAT-MACT, ADMSCs differentiated without triiodothyronine embedded in a peptideless HyA hydrogel; cells-PBS, equivalent number of differentiated ADMSCs delivered in 100 μL PBS. Significance at $^*P < 0.05$, $^{**}P < 0.01$, and $^{***}P < 0.001$.

of our BAT-MACT by allowing us to integrate and independently tune the crosslinking modulus and modulus that cells produce through ligand-specific mechanotransduction observed in Fig. 2*E*.

We have already shown that some ADMSCs spontaneously differentiate into UCP1-expressing cells in vitro using our bio-inspired hydrogel (Fig. 2*F*). In our future studies, generation of UCP1-positive adipocytes could be

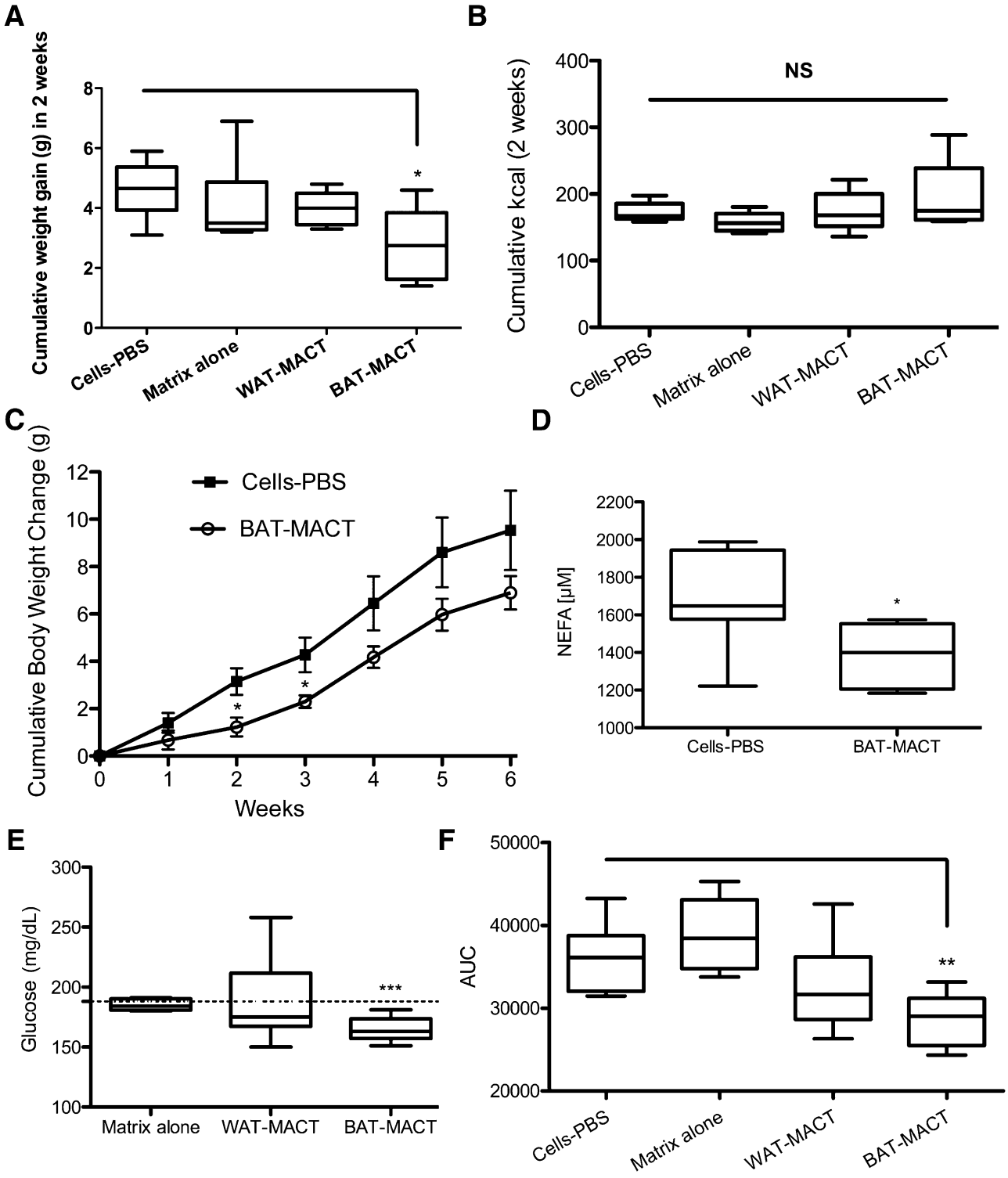

Figure 5—Beige fat expansion promotes improved metabolic profiles in C57BL/6J mice. *A*: Weight gain of mice after 2 weeks of consuming 60% fat diet and being implanted with BAT-MACT or controls receiving cells with no matrix, cell-free matrix, or WAT-MACTs (n = 6). *B*: Cumulative kilocalories consumed by the animals over 2 weeks. NS, not significant. *C*: Body weight of animals injected with matrix-free cells or BAT-MACTs consuming a 60% fat diet over the course of 6 weeks (n = 4). *D*: Serum nonesterified fatty acid (NEFA) concentration. *E*: Resting blood glucose concentrations. *F*: Glucose tolerance test area under curve (AUC) (time points: 0, 20, 30, 60, and 120 min) with an identical dose of glucose given to animals after 2 weeks of consuming 60% fat diet and being implanted with either BAT-MACT or matrix-free control (n = 6). Significance at $^{*}P < 0.05$, $^{**}P < 0.01$, and $^{***}P < 0.001$.

enhanced with matrices presenting heparin-binding growth factors, specifically, BMP7 and FGF21, which have been implicated in BAT differentiation (47). This objective is feasible, as heparin-binding growth factors can be associated with the matrix through the addition of thiolated heparin to the AcHyA (20). Ultimately, there is potential to generate a cell-free matrix that would orchestrate WAT transdifferentiation.

Our current generation of BAT-MACTs was viable for ~30 days in vivo after ~10 days in vitro culture. Duration of the implants is likely determined by a combination of the matrix susceptibility to biodegradation, through the MMP-sensitive crosslinker and HyA backbone, and the life span of brite/beige cells (~50 days) (48). Importantly, we developed MMP-sensitive crosslinkers (30) to enable tissue remodeling and recruitment of host vasculature (Fig. 3*C*). MMP-13 has been shown to be essential for vascularization processes (49), and its expression is one of the most significantly upregulated MMPs during the differentiation of adipocytes (50). Additionally, crosslinkers designed to be sensitive to other MMPs appear to degrade too rapidly in vivo to be used for these applications.

In vivo experiments with BAT-MACTs validated prior notions about the metabolic impact of BAT expansion. Recipients exposed to cold demonstrated that a 100-μL BAT-MACT implant had a significant effect on thermogenesis in a cell-number–dependent manner. BAT-MACTs increased respiration rates and fatty acid utilization, reduced weight gain, and improved glucose homeostasis. These results are in line with recent reports demonstrating that transplantation of primary BAT fragments into mice can prevent diet-induced obesity (10). It remains to be determined whether these beneficial effects are solely due to the increased caloric expenditure afforded by the implant or if they also rely on an endocrine component such as interleukin-6 (10) or other factors secreted by UCP1-positive adipose.

In summary, beige adipose tissue can be engineered using an optimized bio-inspired HyA hydrogel system in conjunction with WAT-derived stem cells and can persist under defined spatio-temporal conditions to affect body temperature, energy homeostasis, weight gain, and insulin sensitivity. These data from our preclinical model demonstrate the feasibility of a novel autologous transplantation-based antiobesity approach with a clear path for ultimate translation into clinical practice. Importantly, the BAT-MACT approach will facilitate systematic evaluation of the metabolic effects of BAT expansion and the underlying biological mechanisms.

Acknowledgments. The authors thank the University of California, Berkeley, imaging core facility members Holly Aaron, Denise Schichnes, and Steve Ruzin for support. The authors also acknowledge Chris Baintner of FLIR for providing thermal imaging equipment.

Funding. This work was supported in part by National Institutes of Health grants R01-DK-101293 and R01-DK-089202 and the American Diabetes Association Basic Science Award 1-14-BS-191 awarded to A.S.

Duality of Interest. No potential conflicts of interest relevant to this article were reported.

Author Contributions. K.M.T. designed and carried out the main experiments with assistance from A.K.J., J.K., and A.Y. A.K.J. designed, produced, and assisted in biomaterials use. G.K., R.S., and E.A.D. designed and produced the FFA-SS-Luc probe. K.E.H. directed and guided bioengineering approaches. A.S. conceived the project, supervised and guided experimental approaches, and wrote the manuscript with assistance from K.M.T. A.S. is the guarantor of this work and, as such, had full access to all the data in the study and takes responsibility for the integrity of the data and the accuracy of the data analysis.

References

1. Rosen ED, Spiegelman BM. What we talk about when we talk about fat. Cell 2014;156:20–44
2. Nicholls DG, Locke RM. Thermogenic mechanisms in brown fat. Physiol Rev 1984;64:1–64
3. Fedorenko A, Lishko PV, Kirichok Y. Mechanism of fatty-acid-dependent UCP1 uncoupling in brown fat mitochondria. Cell 2012;151:400–413
4. Cannon B, Nedergaard J. Brown adipose tissue: function and physiological significance. Physiol Rev 2004;84:277–359
5. Cypess AM, Lehman S, Williams G, et al. Identification and importance of brown adipose tissue in adult humans. N Engl J Med 2009;360:1509–1517
6. van Marken Lichtenbelt WD, Vanhommerig JW, Smulders NM, et al. Cold-activated brown adipose tissue in healthy men. N Engl J Med 2009;360:1500–1508
7. Ma SW, Foster DO. Uptake of glucose and release of fatty acids and glycerol by rat brown adipose tissue in vivo. Can J Physiol Pharmacol 1986;64:609–614
8. Ouellet V, Routhier-Labadie A, Bellemare W, et al. Outdoor temperature, age, sex, body mass index, and diabetic status determine the prevalence, mass, and glucose-uptake activity of ^{18}F-FDG-detected BAT in humans. J Clin Endocrinol Metab 2011;96:192–199
9. Gunawardana SC, Piston DW. Reversal of type 1 diabetes in mice by brown adipose tissue transplant. Diabetes 2012;61:674–682
10. Stanford KI, Middelbeek RJ, Townsend KL, et al. Brown adipose tissue regulates glucose homeostasis and insulin sensitivity. J Clin Invest 2013;123:215–223
11. Ohno H, Shinoda K, Spiegelman BM, Kajimura S. PPARγ agonists induce a white-to-brown fat conversion through stabilization of PRDM16 protein. Cell Metab 2012;15:395–404
12. Elabd C, Chiellini C, Carmona M, et al. Human multipotent adipose-derived stem cells differentiate into functional brown adipocytes. Stem Cells 2009;27:2753–2760
13. Schulz TJ, Huang TL, Tran TT, et al. Identification of inducible brown adipocyte progenitors residing in skeletal muscle and white fat. Proc Natl Acad Sci U S A 2011;108:143–148
14. Ahfeldt T, Schinzel RT, Lee YK, et al. Programming human pluripotent stem cells into white and brown adipocytes. Nat Cell Biol 2012;14:209–219
15. Rodeheffer MS, Birsoy K, Friedman JM. Identification of white adipocyte progenitor cells in vivo. Cell 2008;135:240–249
16. Kajimura S, Seale P, Kubota K, et al. Initiation of myoblast to brown fat switch by a PRDM16-C/EBP-beta transcriptional complex. Nature 2009;460:1154–1158
17. Edelstein ML, Abedi MR, Wixon J, Edelstein RM. Gene therapy clinical trials worldwide 1989-2004-an overview. J Gene Med 2004;6:597–602
18. Huang SJ, Fu RH, Shyu WC, et al. Adipose-derived stem cells: isolation, characterization, and differentiation potential. Cell Transplant 2013;22:701–709
19. Tseng YH, Kokkotou E, Schulz TJ, et al. New role of bone morphogenetic protein 7 in brown adipogenesis and energy expenditure. Nature 2008;454:1000–1004
20. Jha AK, Tharp KM, Ye J, et al. Enhanced survival and engraftment of transplanted stem cells using growth factor sequestering hydrogels. Biomaterials 2015;47:1–12

21. Jha AK, Hule RA, Jiao T, et al. Structural analysis and mechanical characterization of hyaluronic acid-based doubly cross-linked networks. Macromolecules 2009;42:537–546
22. Lee MW, Odegaard JI, Mukundan L, et al. Activated type 2 innate lymphoid cells regulate beige fat biogenesis. Cell 2015;160:74–87
23. Griffith LG, Swartz MA. Capturing complex 3D tissue physiology in vitro. Nat Rev Mol Cell Biol 2006;7:211–224
24. Nakahara H, Nomizu M, Akiyama SK, Yamada Y, Yeh Y, Chen WT. A mechanism for regulation of melanoma invasion. Ligation of alpha6beta1 integrin by laminin G peptides. J Biol Chem 1996;271:27221–27224
25. Nomizu M, Kim WH, Yamamura K, et al. Identification of cell binding sites in the laminin alpha 1 chain carboxyl-terminal globular domain by systematic screening of synthetic peptides. J Biol Chem 1995;270:20583–20590
26. Ponce ML, Nomizu M, Kleinman HK. An angiogenic laminin site and its antagonist bind through the alpha(v)beta3 and alpha5beta1 integrins. FASEB J 2001;15:1389–1397
27. Engler AJ, Sen S, Sweeney HL, Discher DE. Matrix elasticity directs stem cell lineage specification. Cell 2006;126:677–689
28. Shapira-Schweitzer K, Seliktar D. Matrix stiffness affects spontaneous contraction of cardiomyocytes cultured within a PEGylated fibrinogen biomaterial. Acta Biomater 2007;3:33–41
29. Saha K, Keung AJ, Irwin EF, et al. Substrate modulus directs neural stem cell behavior. Biophys J 2008;95:4426–4438
30. Kim S, Chung EH, Gilbert M, Healy KE. Synthetic MMP-13 degradable ECMs based on poly(N-isopropylacrylamide-co-acrylic acid) semi-interpenetrating polymer networks. I. Degradation and cell migration. J Biomed Mater Res A 2005;75:73–88
31. Chung EH, Gilbert M, Virdi AS, Sena K, Sumner DR, Healy KE. Biomimetic artificial ECMs stimulate bone regeneration. J Biomed Mater Res A 2006;79:815–826
32. Wall ST, Yeh CC, Tu RY, Mann MJ, Healy KE. Biomimetic matrices for myocardial stabilization and stem cell transplantation. J Biomed Mater Res A 2010;95:1055–1066
33. Mather BD, Viswanathan K, Miller KM, Long TE. Michael addition reactions in macromolecular design for emerging technologies. Prog Polym Sci 2006;31:487–531
34. Lutolf MP, Raeber GP, Zisch AH, Tirelli N, Hubbell JA. Cell-responsive synthetic hydrogels. Adv Mater 2003;15:888–892
35. Nguyen KD, Qiu Y, Cui X, et al. Alternatively activated macrophages produce catecholamines to sustain adaptive thermogenesis. Nature 2011;480:104–108
36. Guerra C, Koza RA, Yamashita H, Walsh K, Kozak LP. Emergence of brown adipocytes in white fat in mice is under genetic control. Effects on body weight and adiposity. J Clin Invest 1998;102:412–420
37. Stillaert FB, Di Bartolo C, Hunt JA, et al. Human clinical experience with adipose precursor cells seeded on hyaluronic acid-based spongy scaffolds. Biomaterials 2008;29:3953–3959
38. Kim YM, Oh SH, Choi JS, et al. Adipose-derived stem cell-containing hyaluronic acid/alginate hydrogel improves vocal fold wound healing. Laryngoscope 2014;124:E64–E72
39. Henkin AH, Cohen AS, Dubikovskaya EA, et al. Real-time noninvasive imaging of fatty acid uptake in vivo. ACS Chem Biol 2012;7:1884–1891
40. Wu Q, Kazantzis M, Doege H, et al. Fatty acid transport protein 1 is required for nonshivering thermogenesis in brown adipose tissue. Diabetes 2006;55:3229–3237
41. Boss O, Farmer SR. Recruitment of brown adipose tissue as a therapy for obesity-associated diseases. Front Endocrinol (Lausanne) 2012;3:14
42. Xue R, Lynes MD, Dreyfuss JM, Shamsi F, Schulz TJ. Clonal analyses and gene profiling identify genetic biomarkers of the thermogenic potential of human brown and white preadipocytes. Nat Med 2015;21:760–768
43. Wu J, Boström P, Sparks LM, et al. Beige adipocytes are a distinct type of thermogenic fat cell in mouse and human. Cell 2012;150:366–376
44. O'Cearbhaill ED, Ng KS, Karp JM. Emerging medical devices for minimally invasive cell therapy. Mayo Clin Proc 2014;89:259–273
45. Chopra A, Murray ME, Byfield FJ, et al. Augmentation of integrin-mediated mechanotransduction by hyaluronic acid. Biomaterials 2014;35:71–82
46. Bellahcène A, Bonjean K, Fohr B, et al. Bone sialoprotein mediates human endothelial cell attachment and migration and promotes angiogenesis. Circ Res 2000;86:885–891
47. Fisher FM, Kleiner S, Douris N, et al. FGF21 regulates PGC-1α and browning of white adipose tissues in adaptive thermogenesis. Genes Dev 2012;26:271–281
48. Rosenwald M, Perdikari A, Rülicke T, Wolfrum C. Bi-directional interconversion of brite and white adipocytes. Nat Cell Biol 2013;15:659–667
49. Lederle W, Hartenstein B, Meides A, et al. MMP13 as a stromal mediator in controlling persistent angiogenesis in skin carcinoma. Carcinogenesis 2010;31:1175–1184
50. Maquoi E, Munaut C, Colige A, Collen D, Lijnen HR. Modulation of adipose tissue expression of murine matrix metalloproteinases and their tissue inhibitors with obesity. Diabetes 2002;51:1093–1101